



Computational Prediction of the Performance Map of a Transonic Axial Flow Compressor

Moumen Idres^{1,*}, Muhamad Adi Muqri Saiful Azmi¹

¹ Department of Mechanical Engineering, International Islamic University Malaysia, Kuala Lumpur, Malaysia

ARTICLE INFO

Article history:

Received 14 August 2021

Received in revised form 28 February 2022

Accepted 29 February 2022

Available online 31 March 2022

Keywords:

Transonic; compressor; performance map; NASA 37 rotor; Off-design; Flow Separation; ANSYS; CFX

ABSTRACT

Aviation fuel efficiency is an important target for aviation industry. Aircraft engine compression ratio is a key factor to improve fuel consumption. Compression ratio can be increased using transonic compressor. In this study, performance prediction of a transonic axial compressor at design and off-design operating conditions is investigated numerically using ANSYS-CFX software. The compressor is NASA Rotor 37. Firstly, the performance at design point is predicted, where mesh independence study is performed to determine suitable mesh size. Three-dimensional flow details for meridional plane, blade-to-blade plane and airfoil surface are explored. The design point study successfully captured flow features such as shock waves and flow separation regions. When compared with experimental data, the predicted compressor pressure ratio deviation error is less than 5%. 3D flow details show that shock wave strength increases from hub to tip. The shock wave moves backward as we move from hub to tip indicating that the flow separation covers lesser portion of the blade. Secondly, off-design performance is predicted for various rotational speeds. A simple procedure is utilized to predict surge and choke limits. The predicted compressor map is compared with experimental data and it shows overall root mean square error less than 5%. The success of the method developed in this research make it a viable method to be used in the design phase of transonic compressors to evaluate the effect of design modifications for both design and off-design operating conditions.

1. Introduction

Prediction of the performance of turbomachinery is an important step in the design process for many applications [1–3]. For aviation industry, fuel economy is an important objective. Aircraft engine pressure ratio is a key factor that improves fuel efficiency. Transonic compressors are used to achieve high pressure ratio without increase in engine weight [4]. A transonic compressor has a complex flow structure that involves flow separation and shock waves, which requires great care during numerical analysis [5–9]. During early design process, using CFD to analyse performance can save time and cost [10]. During the 1960s, supersonic compressor research flourished with the idea to use a turning blade row followed by an overlapping diamond shaped blade row to avoid suction

* Corresponding author.

E-mail address: midres@iiu.edu.my (Moumen Idres)

side separation of the first blade row is a favourable arrangement for both sub- and supersonic conditions [11].

NASA Rotor 37 was designed as part of a research programme that involved four axial-flow compressor stages intended to cover a range of design parameters typical of aircraft turbine engine high-pressure (core) compressor inlet stages [9,10]. It is a low aspect ratio rotor that is used as a benchmark test case for transonic compressor. It has been investigated experimentally and numerically by many authors [11-16]. Suder *et al.*, [14] investigated experimentally the effect of roughness and coating on the performance. They reported deterioration in performance due to these effects. In a later work, Suder [15] investigated experimentally the impact of the shock/boundary layer interactions and tip clearance on the blockage development. He reported that the blockage in the end wall region is 2-3 times that of the core flow region, and the blockage in the core flow region more than doubles when the shock strength is sufficient to separate the suction surface boundary layer. Dunham [16] studied numerically the effect of the tip gap and made recommendations for grid resolution and turbulence modelling. Ameri [17] used NASA Rotor 37 to validate NASA Glenn-HT code. He reported good agreement with experimental data. Epsipha *et al.*, [18] studied both design and off-design performance of NASA Rotor 37, they showed 3D flow details and performance map. They reported a reduction in efficiency due to the poorly produced shock front for off-design conditions. In a more recent work, Islam and Ma [19] investigated numerically the best locations of probes to reduce the effect on compressor performance during experimental measurements.

Since previous research lacks comprehensive details of the 3D flow structure inside transonic compressors, the current work seeks a comprehensive analysis for both design and off-design conditions with the ultimate goal of generation of the compressor performance map and assessment of accuracy by comparing with experimental data. This comprehensive 3D analysis can be used to evaluate the effect of design modifications on the whole performance map. Ansys [20] software is used to analyse performance of NASA 37 rotor. Both design and off design conditions at 60%, 80% and 100% of design speed are considered. Three-dimensional flow details are explored for the design point case. This includes meridional plane, blade-to-blade plane and airfoil surface. Compressor performance map is obtained and compared with experimental data. A simple procedure to predict surge and choke phenomena is suggested to identify the limits for compressor performance map.

2. Methodology

Simulations are conducted using Ansys software (BladeGen for geometry modelling, Turbogrid for grid generation, CFX for numerical solution, CFX-post for results interpretation). Grid type is structured with hexahedral elements. Flow governing equations are steady-state turbulent ($k-\epsilon$) compressible Reynolds-averaged Navier-Stokes 3D equations.

Blade geometry and domain boundary surfaces are built in BladeGen software. Then, Turbogrid software is used to generate a structured mesh with hexahedral elements. The mesh is clustered near the walls to effectively capture the boundary layer and turbulence. Global sizing factor is used as a mesh clustering parameter to ensure y^+ value near the wall is maintained at 8.8, which is a turbulence modelling requirement. Mesh quality is judged using three factors (skewness, aspect ratio, and smoothness).

The design parameters for NASA Rotor 37 are presented in Figure 1 and Table 1 [17].

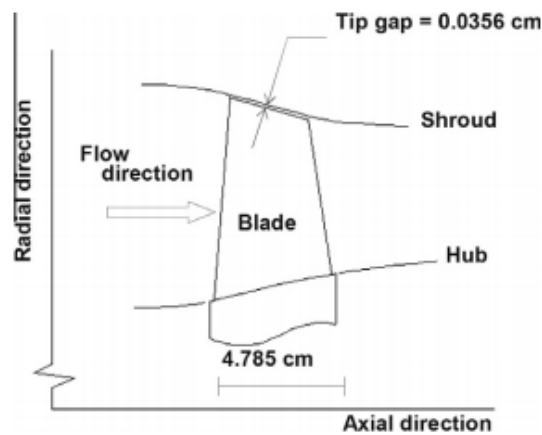


Fig. 1. Meridional view of NASA Rotor 37 [17]

Table 1
 Aerodynamics Design Parameters for NASA Rotor 37 [17]

Variable	Descriptions
Number of blades	36
Blade type	Multiple Circular Arc
Rotational Speed	17188.7 rpm
Inlet hub-tip diameter ratio	0.7
Blade aspect ratio	1.19
Tip solidity	1.29
Tip clearance	0.0356 cm (0.45% of blade span)
Tip speed	454 m/s
Adiabatic efficiency	0.877
Design pressure ratio	2.106
Design mass flow rate	20.19 kg/s
Choked mass flow rate	20.93 kg/s

Figure 2 shows the computational domain. Since, the blade row has 36 blades, a single blade passage occupies a 10° section ($360^\circ/36$). At wall, no slip boundary condition is used. At inlet, total pressure and total temperature are used. At exit, outlet static pressure is imposed. Periodic boundary conditions are imposed at other boundaries of the computational domain. Turbulence intensity was set to 5%. Numerical residuals convergence requirement is set to 1×10^{-6} . Table 2 summarizes computational setup for the design point.

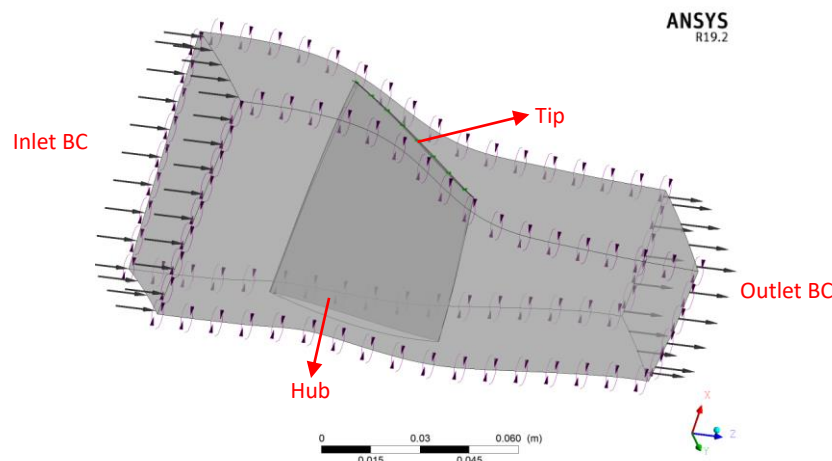


Fig. 2. Computational Domain for NASA Rotor 37

Table 2
 CFX Pre-Setup of NASA Rotor 37

Flow Analysis	
Analysis Type	Steady State
Turbulence Model	K-Epsilon
Equations	RANS
Boundary Conditions	
Wall	No-Slip Wall
Inlet Total Pressure	101.325 kPa
Inlet Total Temperature	288.15 K
Outlet Static Pressure	120 kPa

For performance map prediction, the mesh size determined for the design point is also used for all off-design cases because the design speed is the maximum speed, which needs the maximum mesh size. The rotor speeds used are 100%, 80% and 60% of the design speed. For each rotor speed, several runs for different operating points are obtained by changing outlet static pressure (35 kPa–135 kPa).

3. Results

3.1 Design Point

3.1.1 Mesh independence study

ANSYS Turbogrid is used to generate different meshes required for grid independence study. The Mesh type is structured with hexahedral elements as shown in Figure 3. Global size factor is used as a mesh stretching parameter and hence it can be used to generate different mesh sizes. The y^+ value near the wall is maintained at 8.8, which is a turbulence modelling requirement. As listed in Table 3, four different grids are developed, corresponding to global size factors of 1.3, 1.2, 1.1 and 1. The results of grid independence study is shown in Figure 4. Since computed pressure ratio is almost the same for mesh 3 and mesh 4, mesh 3 is deemed suitable for this study.

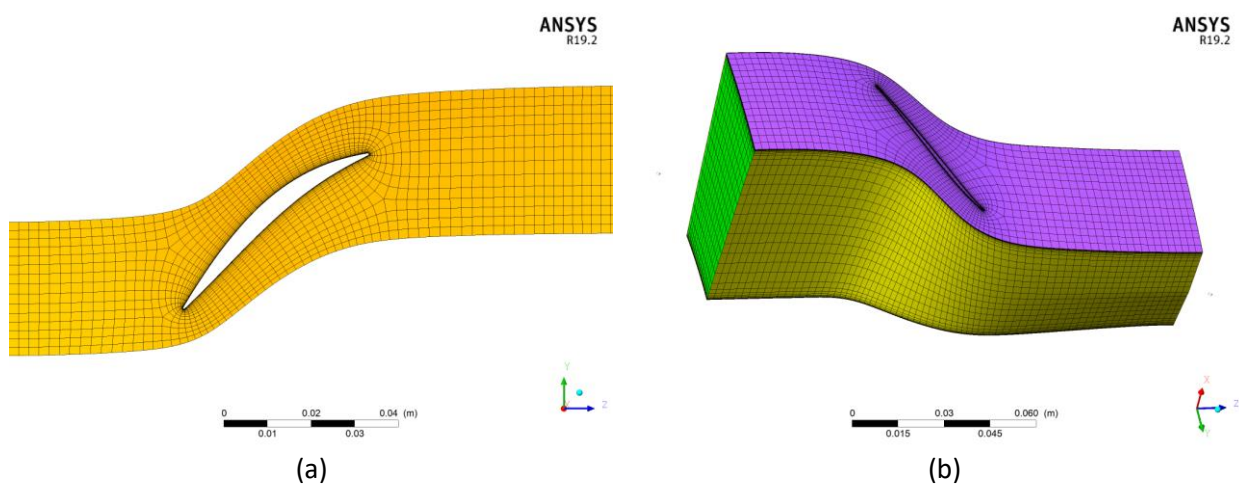


Fig. 3. Mesh details (a) Blade-to-blade (b) 3D view

Table 3
 Mesh independence study

Mesh	Global Size Factor	No of Elements in Spanwise Direction	Total Nodes	Total Elements	Pressure Ratio
Mesh 1	1.3	4	33674	28344	1.9503
Mesh 2	1.2	9	44550	39053	1.9702
Mesh 3	1.1	19	66102	59799	2.0098
Mesh 4	1	38	104666	96258	2.0107

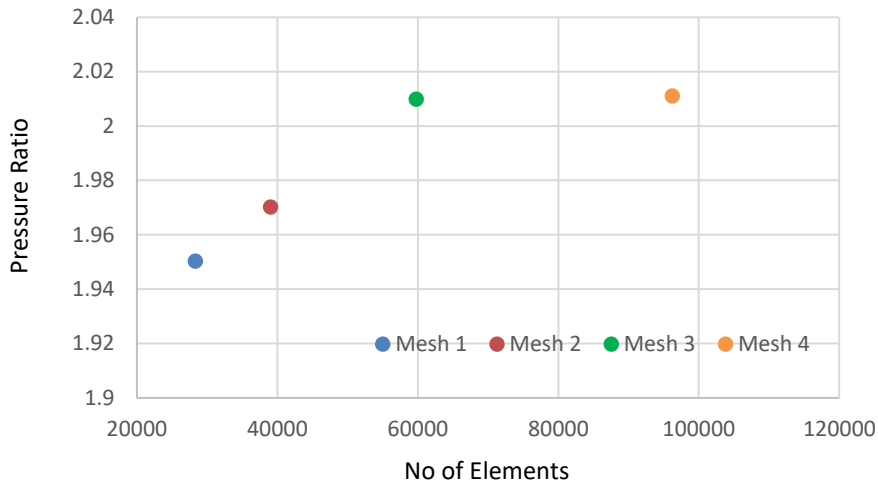


Fig. 4. Mesh Independence Study

3.1.2 Overall results

Table 4 summarizes overall results for the design point. The predicted design point is (20.69, 2.01) to be compared with (20.1, 2.1) from Ameri [17], which leads to an error less than 5%. The design point study serves as a validation study for the computational method and hence the validation is successful.

Table 4
 Overall Performance of NASA Rotor 37

Parameters	Values
Mass Flow Rate, kg/s	20.6949
Volume Flow Rate, m ³ /s	16.8996
Total Pressure Ratio	2.0107
Total Temperature Ratio	1.2623

3.1.3 Meridional plane results

As shown in Figure 5, Meridional plane contours and streamwise plots at spanwise locations of 10%, 50% and 90% of blade span are used to show flow variations through blade passage from leading edge (LE) to trailing edge (TE). Mass-averaged quantities are used. Figure 6(a) depicts mass-averaged pressure contours, where the maximum pressure occurs near the tip of the blade. The contours are almost radial inside blade passage indicating uniform pressure rise in the axial direction. Near trailing edge, pressure rise at the tip is higher than its value at the root. Relative Mach number contours are demonstrated in Figure 6(b), maximum Mach number is 1.5 near to the tip. From LE to TE, relative Mach no. increases then decreases indicating shock wave inside the passage. The shock wave is

shown clearly in the streamwise plot (Figure 7) starting at streamwise location between 0.2 and 0.3 depending on spanwise location (10%, 50%, or 90%).

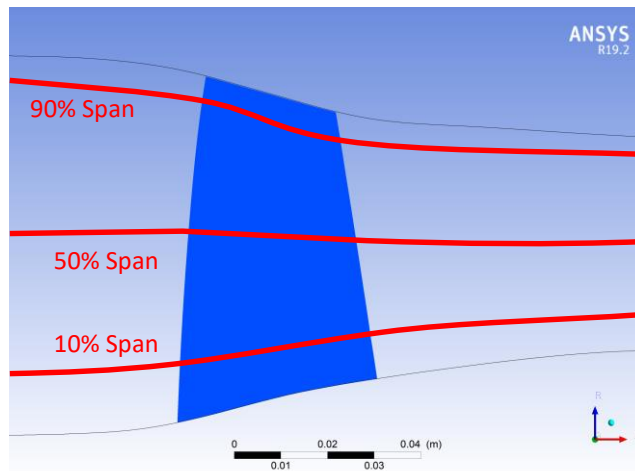


Fig. 5. Meridional plane for NASA Rotor 37

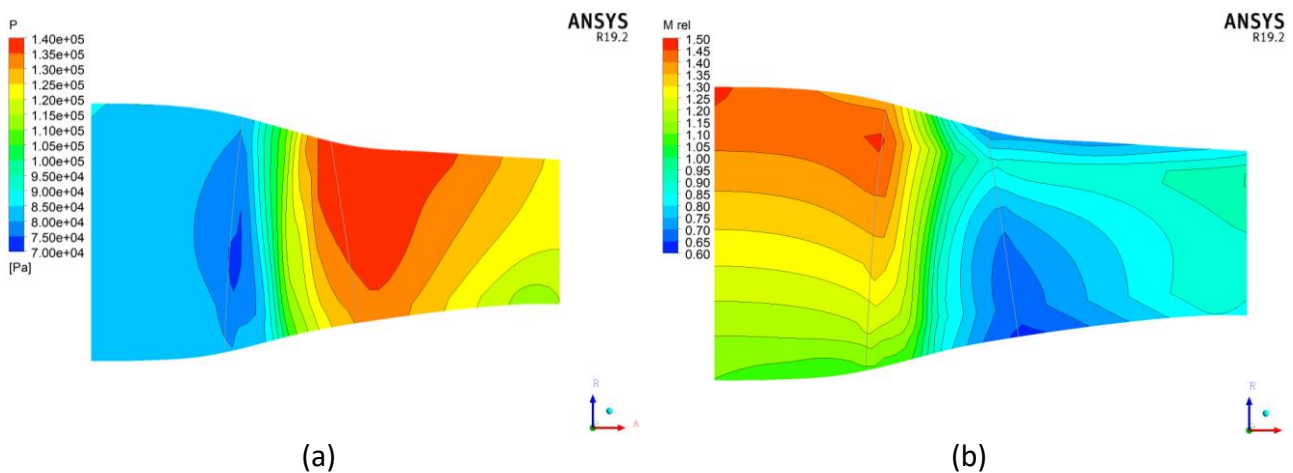


Fig. 6. Meridional plane mass-averaged contours (a) pressure (b) relative Mach no.

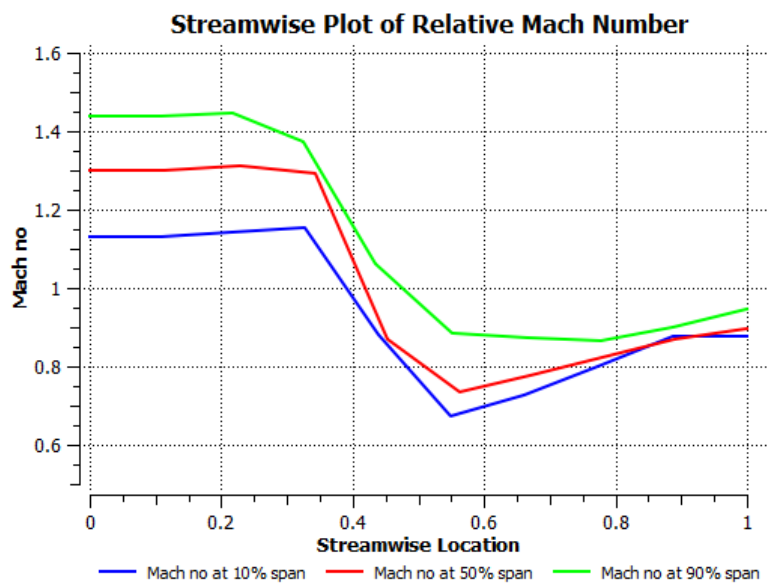


Fig. 7. Streamwise plot for mass-averaged relative Mach no.

3.1.4 Blade-to-blade plane results

Pressure and relative Mach number contours in the blade-to-blade domain at three spanwise locations (10%, 50% and 90% of span) are shown in Figure 8 and Figure 9. At the suction side, in the streamwise direction, flow accelerates where pressure decreases (refer to Figure 8) and relative Mach number increases (refer to Figure 9) until shock wave is formed past middle of the suction side, after which pressure increases and Mach number becomes subsonic. Both figures demonstrate the shock wave locations at the suction side, where shock wave strength increases from hub to tip. This can be inferred from contour spacing at the shock location, where smaller spacing indicates stronger shock. It can be noted that the trailing edge of the blade has the highest value of the pressure. From Figure 9, we can identify flow separation regions at low Mach number areas (blue colour contours) near trailing edge.

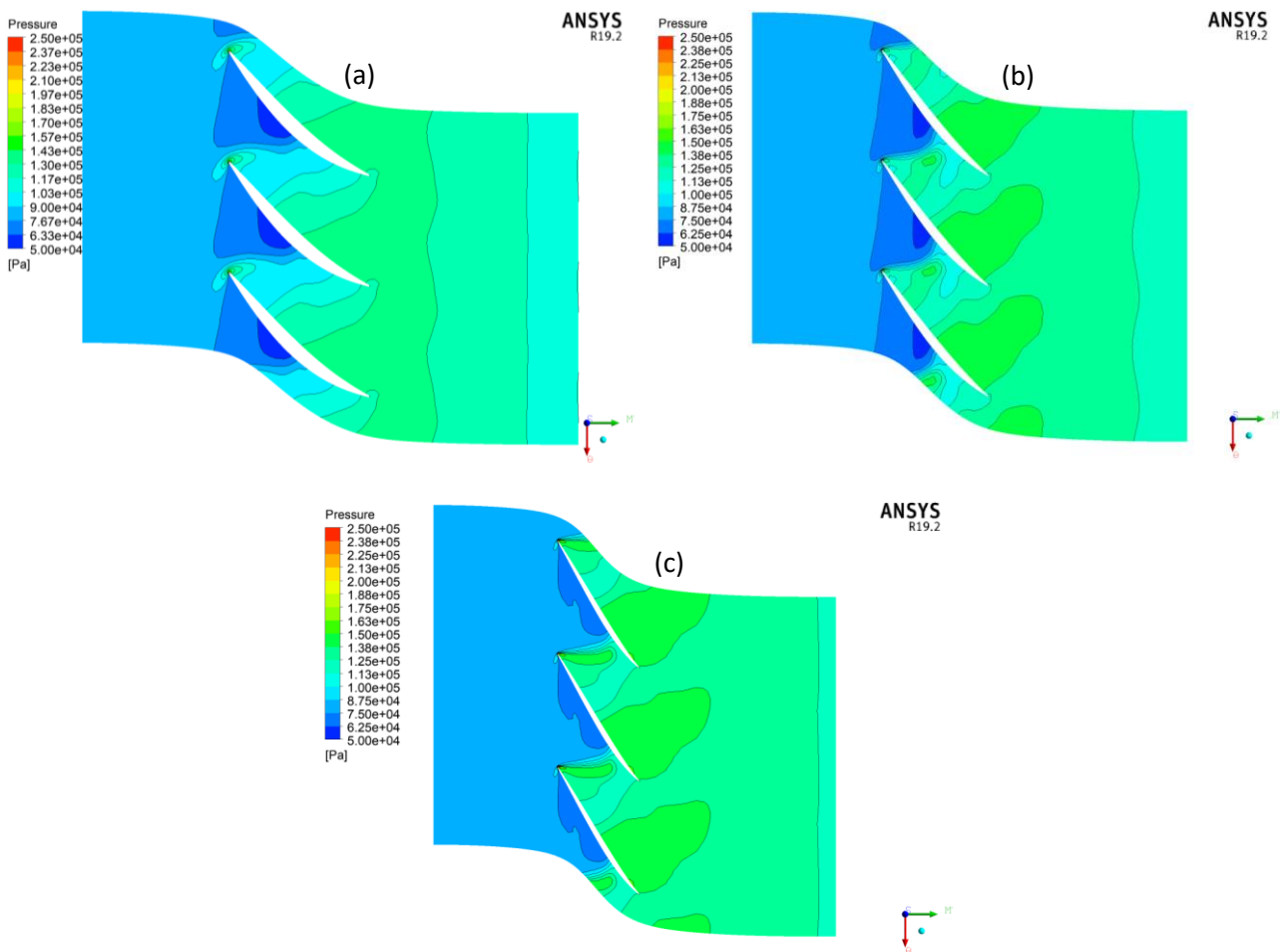


Fig. 8. Blade-to-blade pressure contours at different spanwise locations (a) 10% (b) 50% (c) 90%

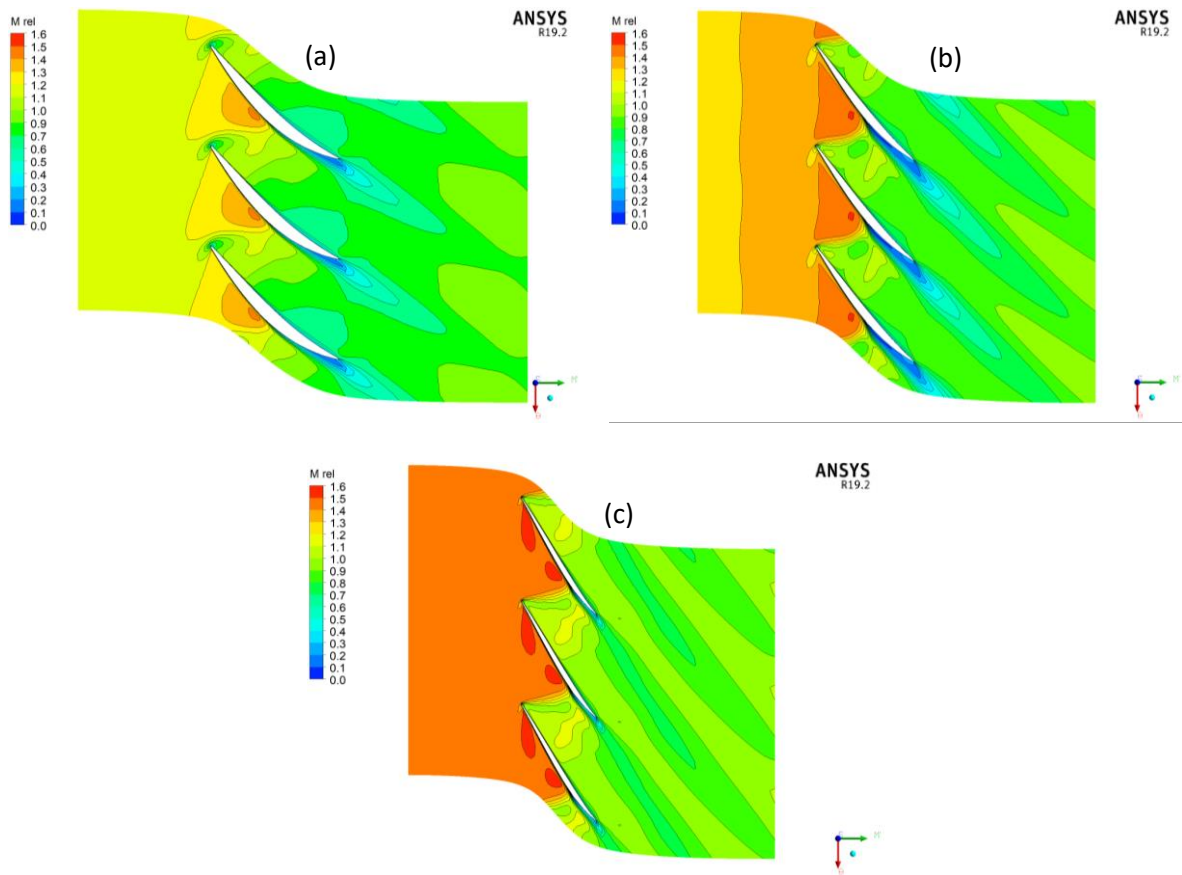


Fig. 9. Blade-to-blade relative Mach number contours at different spanwise locations (a) 10% (b) 50% (c) 90%

3.1.5 Airfoil surface plots

To further investigate the results, plots for airfoil suction-pressure sides are utilized. Figure 10 illustrates pressure distributions around the airfoil sections at spanwise locations 10%, 50% and 90% of the span. At leading edge, there is a large negative pressure gradient (pressure decreases in the streamwise direction) indicating large expansion (flow acceleration). At the suction side (lower pressure curves), shock waves locations are indicated by large positive pressure gradient between streamwise locations 0.4 and 0.7, after which flow separation is expected. This shows that shock wave moves backward as we move from hub to tip indicating that the flow separation covers lesser portion of the blade.

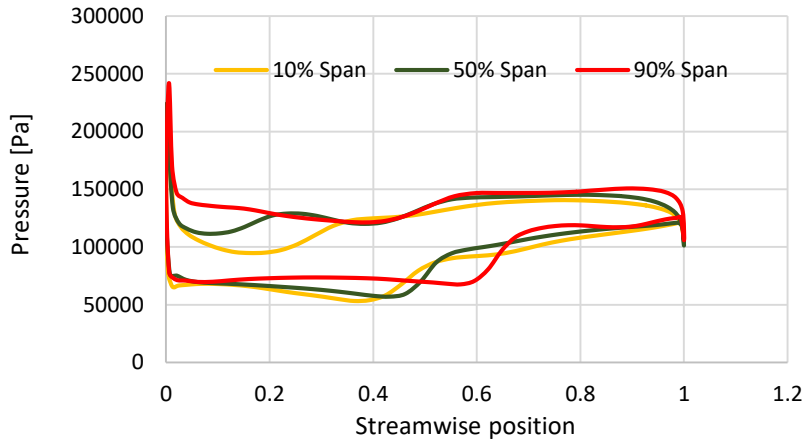


Fig. 10. Airfoil pressure distributions at different spanwise locations

3.2 Performance Map

Figure 11 presents compressor performance map for three speed lines (100%, 80% and 60% of design speed). For each speed line, the limits (minimum mass flow rate and maximum mass flow rates) correspond to surge condition (minimum mass flow rate and maximum pressure ratio) and choking condition (maximum mass flow rate and minimum pressure ratio). Surge is an unsteady phenomenon where mass flow rate is oscillating. It cannot be predicted using current method. Numerical solution convergence is used as a simple criterion to indicate nearness to surge. So, to approximately determine surge limit, exit pressure is decreased till numerical solution convergence is failing. For choking limit, exit pressure is increased slowly till speed line becomes almost vertical. To assess overall accuracy of calculation, overall root mean square error (ORMSE) is calculated using all speed lines. To calculate overall root, mean square error, we calculate the average square error (the summation of the squares of the differences between computed values and experimental values divided by total number of points), then, we take the root of the resulting value. The resulting ORMSE is 3.54%, which demonstrates acceptable accuracy.

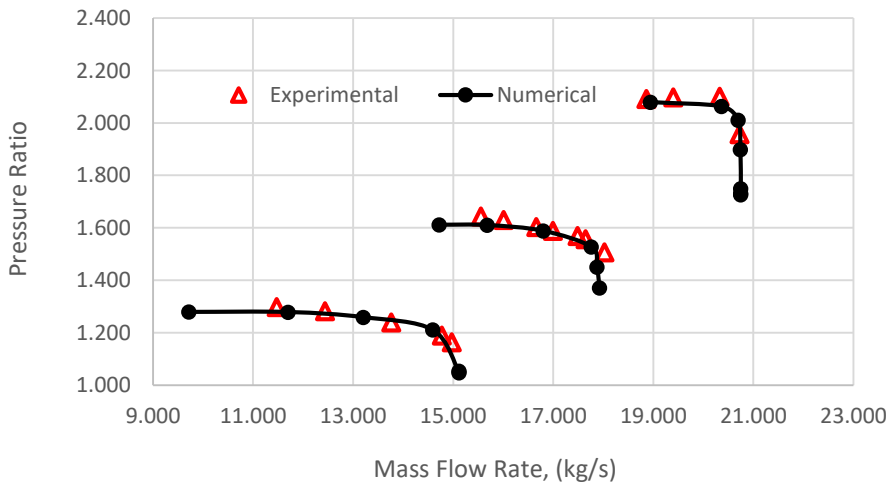


Fig. 11. NASA Rotor 37 Performance Map

4. Conclusions

Ansys-CFX CFD simulations were conducted for a transonic axial flow compressor rotor at the design and off-design conditions. The method is based on turbulent RANS 3D equations. Comprehensive 3D results are presented for the design case. This includes meridional plane, blade-to-blade plane and airfoil distribution plots and contours. It shows the capability to capture shock waves and flow separation. Compressor performance map is predicted, where surge and choking limits are estimated. The results are compared with experimental data for both design and off-design cases. Overall error is less than 5%. Current method can be used in the design phase to predict the effect of geometry and/or flow changes on the performance of the compressor.

Acknowledgement

This research was funded by International Islamic University Malaysia.

References

- [1] Mobarak, Amin, Mostafa Shawky Abdel Moez, and Shady Ali. "Quasi Three-Dimensional Design for a Novel Turbo-Vapor Compressor and the Last Stage of a Low-Pressure Steam Turbine." *Journal of Advanced Research in Fluid Mechanics and Thermal Sciences* 85, no. 2 (2021): 1-13. <https://doi.org/10.37934/arfmts.85.2.113>
- [2] Jawad, Layth H., Shahrir Abdullah, Rozli Zulkifli, and Wan Mohd Faizal Wan Mahmood. "Numerical investigation on the effect of impeller trimming on the performance of a modified compressor." *CFD Letters* 5, no. 4 (2013): 174-184.
- [3] Gurnathan, Balamurugan A., Uswah Khairuddin, Nazrun Nabill Azlan Shah, and Ricardo Martinez-Botas. "Influence of Double Entry Volute on Incidence Angle Variation Under Steady Flow: Numerical Investigation." *CFD Letters* 12, no. 10 (2020): 75-89. <https://doi.org/10.37934/cfdl.12.10.7589>
- [4] Hawthorne, William R., ed. *Aerodynamics of Turbines and Compressors*. (HSA-1), Volume 1. Vol. 5204. Princeton University Press, 1964. <https://doi.org/10.1515/9781400885985-003>
- [5] Biollo, Roberto, and Ernesto Benini. "Recent advances in transonic axial compressor aerodynamics." *Progress in Aerospace Sciences* 56 (2013): 1-18. <https://doi.org/10.1016/j.paerosci.2012.05.002>
- [6] Tyacke, James, N. R. Vadlamani, W. Trojak, R. Watson, Y. Ma, and P. G. Tucker. "Turbomachinery simulation challenges and the future." *Progress in Aerospace Sciences* 110 (2019): 100554. <https://doi.org/10.1016/j.paerosci.2019.100554>
- [7] Hergt, Alexander, Joachim Klinner, Jens Wellner, Christian Willert, Sebastian Grund, Wolfgang Steinert, and Manfred Beversdorff. "The present challenge of transonic compressor blade design." *Journal of Turbomachinery* 141, no. 9 (2019). <https://doi.org/10.1115/1.4043329>
- [8] Pinto, Runa Nivea, Asif Afzal, Loyan Vinson D'Souza, Zahid Ansari, and AD3657327 Mohammed Samee. "Computational fluid dynamics in turbomachinery: a review of state of the art." *Archives of Computational Methods in Engineering* 24, no. 3 (2017): 467-479. <https://doi.org/10.1007/s11831-016-9175-2>
- [9] Nel, Philip. "Computational fluid dynamics-modelling of a multi-stage transonic axial-flow compressor." *PhD diss., Stellenbosch: Stellenbosch University*, 2017.
- [10] Li, Zhihui, and Xinqian Zheng. "Review of design optimization methods for turbomachinery aerodynamics." *Progress in Aerospace Sciences* 93 (2017): 1-23. <https://doi.org/10.1016/j.paerosci.2017.05.003>
- [11] Broichhausen, Klaus D., and Kai U. Ziegler. "Supersonic and transonic compressors: past, status and technology trends." In *Turbo Expo: Power for Land, Sea, and Air*, vol. 47306, pp. 63-74. 2005. <https://doi.org/10.1115/GT2005-69067>
- [12] Reid, Lonnie, and Royce D. Moore. *Design and overall performance of four highly loaded, high speed inlet stages for an advanced high-pressure-ratio core compressor*. No. NASA-TP-1337. 1978.
- [13] Reid, Lonnie, and Royce D. Moore. "Experimental study of low aspect ratio compressor blading." *Journal of Engineering for Gas Turbines and Power* 102, no. 4 (1980): 875-882. <https://doi.org/10.1115/1.3230353>
- [14] Suder, Kenneth L., Rodrick V. Chima, Anthony J. Strazisar, and William B. Roberts. "The effect of adding roughness and thickness to a transonic axial compressor rotor." In *Turbo Expo: Power for Land, Sea, and Air*, vol. 78835, p. V001T01A113. American Society of Mechanical Engineers, 1994. <https://doi.org/10.1115/94-GT-339>
- [15] Suder, Kenneth L. "Blockage development in a transonic, axial compressor rotor." *Journal of Turbomachinery* 120, no. 3 (1998): 465-476. <https://doi.org/10.1115/1.2841741>
- [16] Dunham, John. *CFD Validation for Propulsion System Components (la Validation CFD des organes des propulseurs)*.

Advisory Group For Aerospace Research And Development Neuilly-Sur-Seine (France), 1998.

- [17] Ameri, Ali A. *NASA Rotor 37 CFD Code Validation*. NASA CR-216235, National Aeronautics and Space Administration, Glenn Research Center, 2010. <https://doi.org/10.2514/6.2009-1060>
- [18] Epsipha, Pauline, Z. Mohammad, and A. A. Kamarul. "CFD investigation of transonic axial compressor rotor blade at various off-design conditions." *Pertanika Journal of Science and Technology* 24, no. 2 (2016): 451-463.
- [19] Islam, Asad, and Hongwei Ma. "Numerical study of probe parameters on performance of a transonic axial compressor." *PLoS ONE* 16, no. 1 (2021): e0245711. <https://doi.org/10.1371/journal.pone.0245711>
- [20] Ansys. "Ansys CFX." *Ansys, Inc.* 2022. <https://www.ansys.com/products/fluids/ansys-cfx>.